JMEPEG (2012) 21:2684–2690
DOI: 10.1007/s11665-012-0376-z

1059-9495/$19.00

Microstructure and Properties of Deformation Processed Polycrystalline $Ni_{47}Ti_{44}Nb_9$ Shape Memory Alloy

XiangQian Yin, Xujun Mi, Yanfeng Li, and Baodong Gao

(Submitted March 15, 2012; in revised form August 8, 2012)

The objective of this work was to investigate the relationships between process and microstructure and property in polycrystalline $Ni_{47}Ti_{44}Nb_9$ alloy. Three processes: (1) hot-forged, (2) cold-drawn, and (3) cold-rolled were investigated. The microstructure was tested by means of optical microscope, x-ray diffraction, and electron backscatter diffraction, and then crystalline orientation distribution functions and inverse pole figures were measured. The results indicated that hot-forging eliminated dendritic microstructure and fined the eutectic structure. It also induced a ⟨113⟩ fiber texture, which paralleled to the axial direction. The cold drawing and cold-rolling had a further effect in grain refinement. And the cold-drawn specimens contained a strong ⟨111⟩ fiber texture paralleling to the deformation direction, while the cold-rolled tubes formed ⟨111⟩ crystalline directions paralleling the axial direction and ⟨110⟩ crystalline directions of crystalline arranged along the circumferential direction. The notably distinctive recoverability of different processed materials was observed and discussed.

Keywords deformation process, NiTiNb alloy, pipe coupling, texture

1. Introduction

Shape memory alloys (SMAs) such as nickel-titanium (NiTi) have a special capability to recover large strain induced by mechanical deformation. This capability is sufficiently exploited in many SMA applications (e.g., pipe couplings). As is well known, the TiNiFe alloy pipe coupling is widely used in aviation industry. Due to the low martensitic transformation temperature and narrow thermal hysteresis, the TiNiFe pipe coupling must be stored in liquid nitrogen. Many recent researches show that NiTiNb alloys have good mechanical properties, suitable martensitic transformation temperature, and very wide thermal hysteresis (Ref 1, 2). So, if pipe couplings can be made of NiTiNb alloy, it will be stored and transported conveniently at room temperature. And many researchers have started to exploit the potentiality of NiTiNb alloys (Ref 3-5).

Like other NiTi-based alloys, the recoverability of NiTiNb alloy is fulfilled when martensite variants return to the austenite. During the phase transformation, monoclinic martensite phase (B19′) with low symmetry converts to high-symmetry body-centered cubic (bcc) austenite phase (B2) (Ref 6). Therefore, different lattice orientations lead to distinct recoverability. Several experiments focusing on single crystal have shown that different martensitic transformation behaviors depended on crystallographic orientations (Ref 7-9). Following studies showed that textures played similar roles in processed polycrystalline NiTi alloys (Ref 10, 11). Miyazaki et al. examined the textures of cold-rolled NiTi thin plates, and discussed quantification of the relationship between transformation strain and crystal orientation (Ref 12). Texture and shape memory property of melt-spun TiNiCu ribbons (Ref 13) and hot-rolled TiNi bars (Ref 14) were also investigated.

In these foregoing studies, they usually focused on isolated relationships between crystallographic textures and transformation behaviors of single deformation processed NiTinol materials. In practice, deformation processes such as forging, drawing, and rolling are always used in combination, and the main object of deformation processes is to obtain appropriate microstructure and material size. Furthermore, most previous researches concentrated on thin sheets (Ref 12, 15, 16) or bars (Ref 17) rather than tubes which were widely used in engineering. In this paper, three different processes were investigated, and the study focused on understanding the fundamental physical links between processing, microstructure, and relevant properties. The notable difference of recoverability in two contrasting tube process flows was also observed and discussed.

2. Experimental Procedures

2.1 Materials and Specimens

Consumable electrode arc melting was used to produce $Ni_{47}Ti_{44}Nb_9$ (at.%) ingot with a diameter of 200 mm, and then the ingot undergone cogging and multi-direction forging with 50% reduction per pass at 950 °C. Then we got 50-mm diameter rods (denoted as: original NiTiNb materials). After sampling, these rods were divided into two batches. With 20%

This article is an invited paper selected from presentations at the International Conference on Shape Memory and Superelastic Technologies 2011, held November 6-9, 2011, in Hong Kong, China, and has been expanded from the original presentation.

XiangQian Yin, Xujun Mi, Yanfeng Li and **Baodong Gao**, State Key Laboratory of Nonferrous Metals and Processes, General Research Institute for Nonferrous Metals, Beijing, China. Contact e-mails: yinxiangqianbj@gmail.com and yinxq@ymail.com.

reduction per pass at 850 °C, one batch of rods was hot-forged down to 12-mm diameter rods (denoted as: hot-forged NiTiNb materials). Those 12-mm diameter rods were cold-drawn, then annealed at 650 °C for 0.5 h, and finally cold-drawn down to 8-mm diameter bars (denoted as: cold-drawn NiTiNb materials). While another batch, with a pre-manufactured hole, was processed by cold three-roll rolling processes with intermediate annealing, and then obtained tubes with an external diameter of 8 mm and a wall thickness of 2 mm (denoted as: cold-rolled NiTiNb materials). The specimens were cut by spark cutting and heat treated at 850 °C for 1 h in an evacuated quartz tube. The normal direction (ND) of x-ray diffraction (XRD) and EBSD test zone paralleled the axial direction of rods or tubes.

2.2 Test Methods

Specimens for XRD were mechanically polished and then for tested by a Philips X' Pert MRD XRD machine. Cu Kα X-ray was used at 40 kV, 40 mA, and with a scanning range of 20°-85°. The XRD pattern of NiTiNb alloy was shown in Fig. 1. Texture data were obtained from {110}, {200}, and {211} planes in the B2 parent phase and characterized in the form of orientation distribution functions (ODFs).

The mechanical polished specimens were then etched using a solution consisting of 10 mL HF and 30 mL HNO_3 and 100 mL H_2O for 30 s. This etchant preferentially attracts on grain boundaries which consisted by eutectic structure, but does not result in their crystallographic grain boundary. So the metallography calculated from EBSD (Fig. 2) is different to optical micrography (Fig. 3c).

Specimens for electron backscatter diffraction (EBSD) were mechanically polished followed by electrolytic polishing. The electrolyte solution was a mixture of 25% HNO_3 and 75% methanol. The electrolytic polishing was conducted at 18 V in electrolyte solution with a temperature of −40 °C (Ref 18). A JEOL 6700 field emission SEM equipped with a backscattering diffraction detector was used for EBSD test. Crystallographic orientations were obtained by indexing of Kikuchi patterns with TSL-EDAX software. For convenient analysis, the ND of EBSD test zones paralleled the axial direction of pipe couplings, while the transverse direction (TD) paralleled along the circumferential direction.

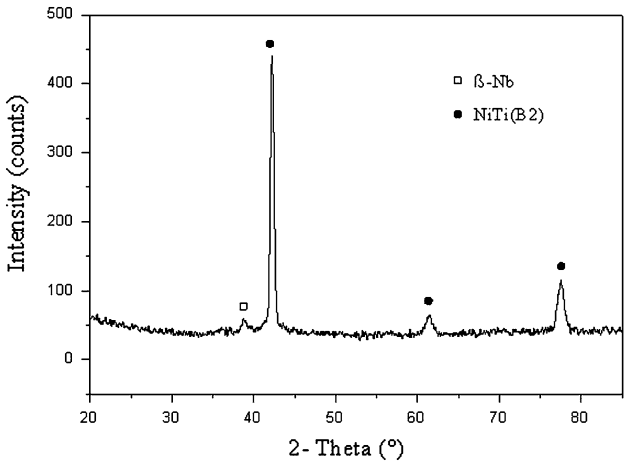

Fig. 1 XRD diffraction patterns of hot-forged NiTiNb alloy with β-Nb and austenite (B2) peaks identified

The shape memory property of cold-drawn and cold-rolled materials was characterized by inner diameter recoverability of corresponding pipe couplings. The pipe couplings, with an inner diameter of 4 mm, a wall thickness of 1.8 mm, and a length of 16 mm, were machined by cold-drawn ribbons or cold-rolled tubes. Those pipe couplings were heat treated at 850 °C for 1 h in an evacuated quartz tube, and then were enlarged at −60 °C with an expanding ratios of 1.16. After the inner diameter (Φ_1) was measured, the pipe coupling was heated to 100 °C for 5 min in water bath to obtain a completely inverse martensitic transformation. Then the inner diameter (Φ_2) was measured again. The recoverability (η) of pipe coupling was calculated according to the following formula: $\eta = (\Phi_1 - \Phi_2)/\Phi_1$.

3. Results

3.1 Microstructure of Deformed Materials

The optical metallography of NiTiNb alloy in different deformation states (original materials, hot-forged materials, cold-drawn materials, and cold-rolled materials) were shown in Fig. 3(a-d). According to the XRD for phase identification as shown in Fig. 1, the microstructure was consisted of TiNi matrix phase that was bright in the micrography and eutectic structure comprising β-Nb particles that had been etched off (Ref 19, 20). The grain size of original and hot-forged NiTiNb material was about 10-20 μm, while both cold-rolled and cold-drawn NiTiNb material was about 5-10 μm. The eutectic structure displayed a similar change. Cold-working material (cold-drawn and cold-rolled material) has much finer and more dispersed eutectic structure than hot-working (original and hot-forged material) material. Otherwise, only the original material exhibited dendritic microstructure in the center of rods, which was circled in Fig. 3(a).

3.2 Texture After Deformation

Figure 4 showed that the original materials possessed mixed fiber texture of ⟨113⟩ (5-6 times random) and ⟨331⟩ (1-1.5 times random). The texture of hot-forged materials was clear fiber texture in ⟨113⟩ direction and it was 15 times random as shown in Fig. 4(b).

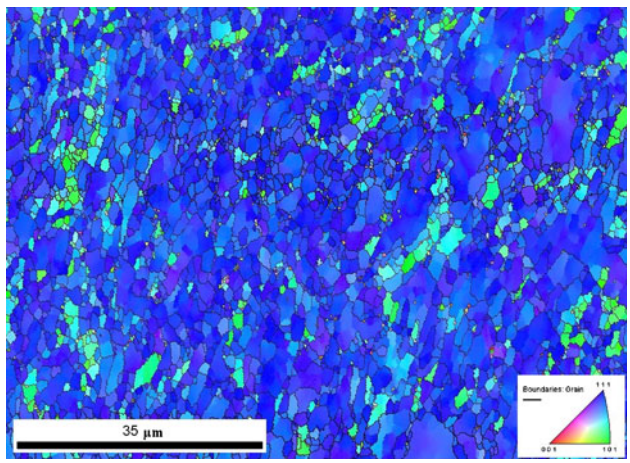

Fig. 2 Three-color EBSD map of cold drawn materials

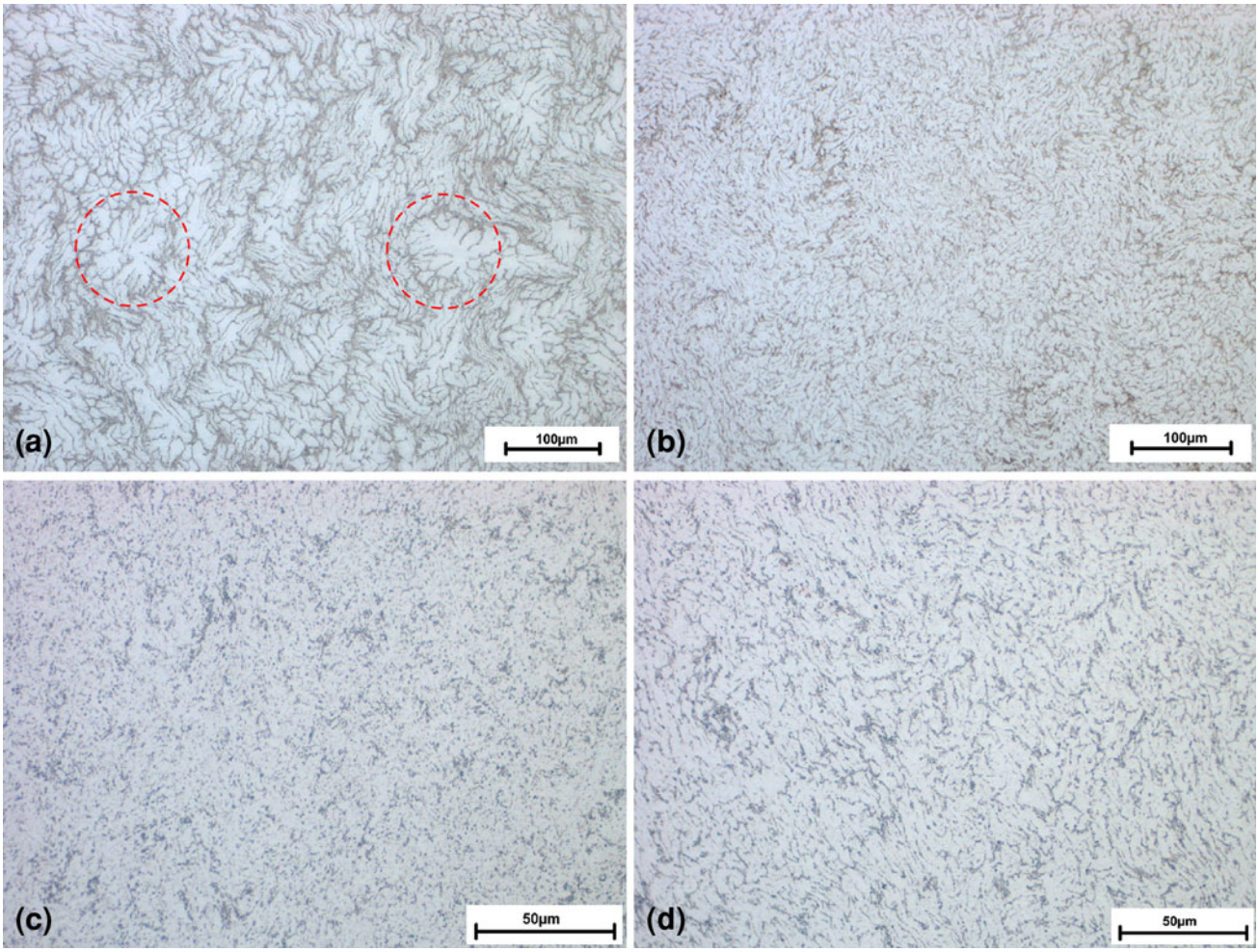

Fig. 3 Optical metallography of $Ni_{47}Ti_{44}Nb_9$ alloy (a) original materials, (b) hot-forged materials, (c) cold-drawn materials, (d) cold-rolled materials

The inverse pole figures (IPFs) of cold-drawn and cold-rolled materials were shown in Fig. 5, which were calculated by EBSD. In Fig. 5(a), there was high density preferred orientation in ⟨111⟩ district of ND IPF and ⟨110⟩ district of TD IPF, which indicated that ⟨111⟩ crystal directions paralleled to axial direction and ⟨110⟩ crystal directions paralleled to circumferential direction of cold-rolled tubes. Compared with cold-rolled materials, the density of ⟨111⟩ texture was higher in the cold-drawn specimens (as high as 18 times random) in ND IPF, but the preferred orientation was weaker and undisciplined in TD IPF as shown in Fig. 5(b). It means that cold-drawn tubes contained stronger ⟨111⟩ texture paralleled to axial direction and weaker ⟨110⟩ texture paralleled to circumferential direction than cold-rolled tubes.

3.3 Recoverability of Materials

The recoverability of 50 pieces cold-drawn and 50 pieces cold-rolled pipe couplings were measured. And the average recoverability (η) of cold-drawn pipe coupling was 7.1%, while the cold-rolled pipe coupling was 8.4%, as showed in Fig. 6. With uniform size and the same expanding diameter process, this result reflected that cold-rolled materials had higher circumferential recoverability than cold-drawn materials.

4. Discussions

The experimental results showed the effects of deformation processes on microstructure, texture, and recoverability. The relationship of processing-microstructure-property is discussed as following.

4.1 Effects of Deformation Processes on Microstructure

Some studies show the grain size and metallography of SMAs with different deformation processes (Ref 20-22). In this study, the 50-mm diameter original rods are produced from an ingot of 200 mm in diameter. Due to the preceding hot-working, grain size of original material is more fined than some of previous reports (Ref 17, 23). However, the grain refinement in following hot-forging processes (50-mm rods hot-forged down to 12-mm rods) is limited. Basing on our previous study (Ref 24), dynamic recrystallization might occurred in cogging and multi-direction forging with 50% reduction per pass at 950 °C, while dynamic recovery might be the major soften mechanism in following hot-forging process with 20% reduction per pass at 850 °C.

The micro-morphology of original and hot-forged materials also showed great difference. As for large material size causing

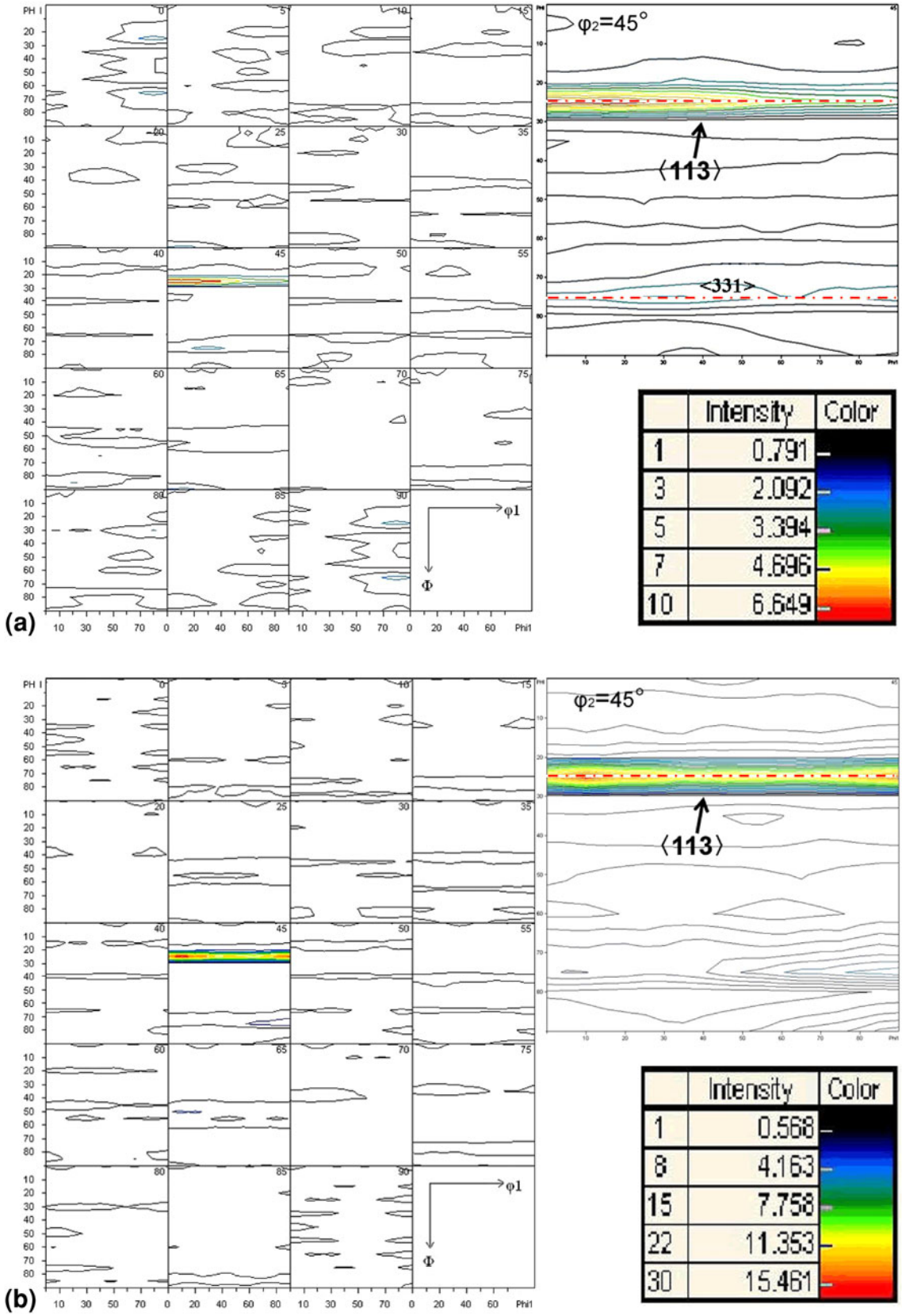

Fig. 4 ODF sections and the ODF section at φ_2=45° of (a) original NiTiNb materials and (b) hot-forged NiTiNb materials, revealing both NiTiNb materials contained a ⟨113⟩ fiber texture

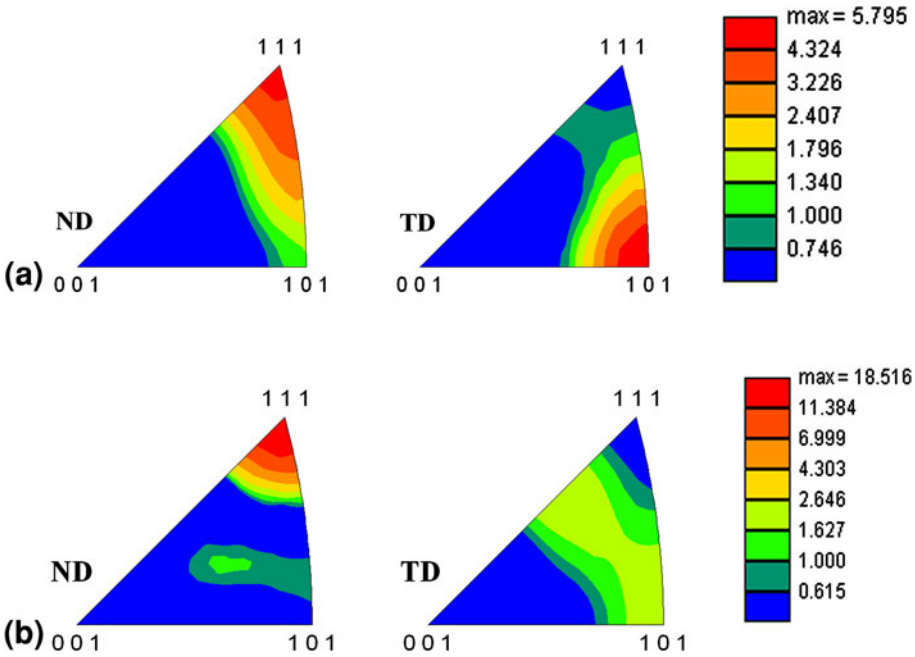

Fig. 5 IPF of the (a) cold-rolled and (b) cold-drawn NiTiNb materials, representing the preferred crystalline orientation in the axial direction (ND of specimen) and circumference direction (TD of specimen)

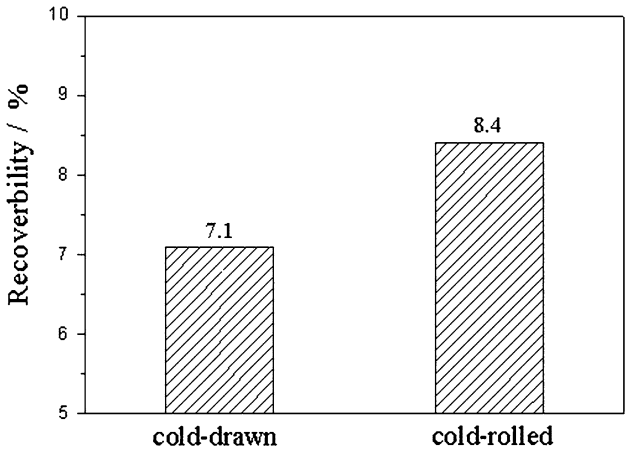

Fig. 6 Recoverability of cold-drawn and cold-rolled pipe couplings

uneven deformation, original materials contain some dendritic microstructure in the center of original rods (Fig. 3a). This dendritic microstructure causes the nonuniformity of elongation. With following hot-forgings, dendritic microstructure is eliminated, and eutectic structure turns into fined and dispersed which is advantageous to mechanical properties. Table 1 showed that hot-forged materials have higher strength and elongation than original materials. The homogeneous properties and higher elongation are the most important factors for cold workability. So, for NiTiNb alloy, hot-forging processes not only provide semi-manufacture in suitable material dimension, but also benefit for attaining dispersed and homogeneous microstructure for following cold processes, which is same with other NiTi alloys (Ref 25).

As shown in Fig. 3(c) and (d), the grain size of cold-workings (cold-drawn and cold-rolled materials) decreases to 5-10 μm, which is far more fined than hot-forged. The cold-working induces high-density dislocation walls and microbands, as shown in Fig. 7(a). With heating treatment, the dislocation walls and microbands develops to low angle grain boundaries or to trigger recrystallization (as Fig. 7(b) shows). And then, the grain boundary migrates and crystalline grain grows. After the heat treatment, cold worked materials get full static recrystallization (as Fig. 2 shows), and showed similar microstructure in grain size and micro-morphology both in cold-drawn and cold-rolled materials.

4.2 Effects of Deformation Processes on Texture

Deformation processes have an obvious influence on textures as well as the metallography. The texture of ingot induced by temperature-gradient-driven is always random and strong (Ref 17). Due to analogical deformation processes, both the original and hot-forged materials show a clear ⟨113⟩ fiber texture as Fig. 4(a) and (b). But the ⟨113⟩ texture density of hot-forged material was increased to 15 times random. It infers that ⟨113⟩ texture is induced and intensified by hot forging processes.

After cold-working, the texture is changed. Both cold-drawn materials possess a strong ⟨111⟩ preferred orientation paralleling to the axial direction. But in circumference direction (TD), only cold-rolled materials exhibit a clear preferred orientation in ⟨110⟩ district. This crystal orientation is dependent upon the tube deformation mode. With three-roll rolling processes, not only the axial direction but also the direction along the thickness of the tube undergoes deformation. Generally, this axisymmetrical tube deformation is between extreme cases of drawing and sheet rolling (Ref 26, 27). Accordingly, the cold-rolled tubes form ⟨111⟩ texture in the axial direction, which is similar to the cold-drawn materials, and while it also develops ⟨110⟩ crystalline orientation preferred along the circumferential direction, which exists in cold flat rolling sheets (Ref 28, 29).

Table 1 Experimentally measured mechanical properties of hot-forged NiTiNb rods (without heat treatment)

Materials	Fracture strength, MPa	Yield strength, MPa	Elongation to fracture, %
50-mm rod center	770	485	32.5
50-mm rod 1/2 radial point	768	470	43.0
50-mm rod edge	785	473	37.5
12-mm bar center	791	487	61.0
12-mm bar edge	802	492	57.8

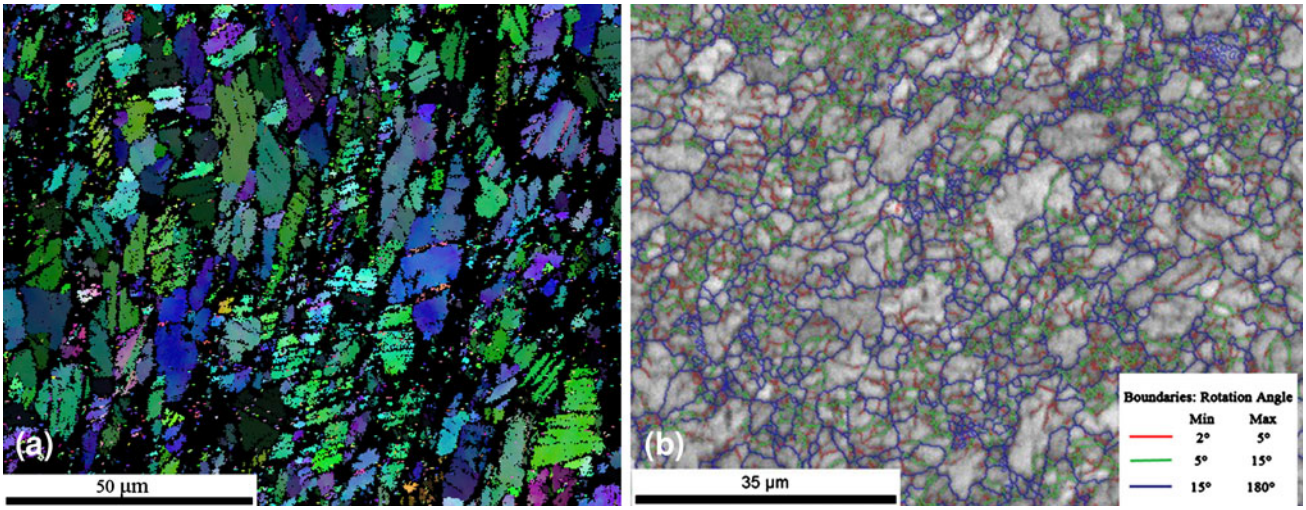

Fig. 7 EBSD maps of NiTiNb alloy, (a) cold-rolled, the black district presenting the severe plastic deformation area and (b) cold-rolled and then annealed at 600 °C for 30 min, showing different rotation angle boundaries

4.3 Effects of Texture on Recoverability

The mathematic relationship between transformation strain and crystal orientation is calculated by crystallographic point of view called "phenomenological crystallographic theory" in single crystal. Based on the theory, the transformation strain produced by lattice distortion during martensitic transformation can be calculated by lattice constants (Ref 6, 8, 12, 28). As shown in Fig. 8, the above quantitative relationships could be well expressed in [001]-[011]-[111] standard stereographic triangle, which shows that the calculated recovery strain was dependent on orientation. The recoverable strain would increase if the crystal axis was preferentially located around the [011] or [111] district, while it is relatively small if the crystalline aligned along the [001] direction. The following studies showed that it also fit to polycrystalline NiTi thin films and sheets (Ref 6, 12, 28). As for pipe couplings, it should be analyzed in cylindrical coordinate. With inner diameter Φ increasing to Φ_1, the mechanical strain ε is induced in circumference direction,

$$\varepsilon = \frac{2\pi(\Phi_1 - \Phi)}{2\pi\Phi} = \frac{\Phi_1 - \Phi}{\Phi}.$$

During inverse martensitic transformation, circumferential strain ε recovered and inner diameter Φ_1 decreases to Φ_2. Thus, the recoverability of pipe couplings η depended on the recoverability of circumferential strain ε, which is affected by preferred orientation in the circumferential direction.

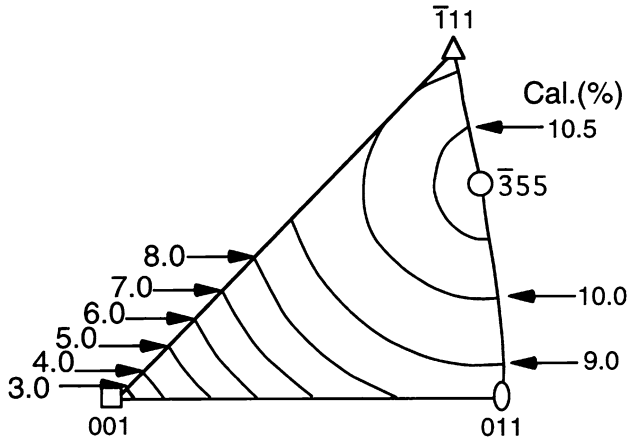

Fig. 8 Orientation dependence of the calculated transformation strain associated with the martensitic transformation (Ref 7)

As shown in Fig. 5, the cold-rolled materials possess $\langle 110 \rangle$ crystal preferred orientation in the circumferential direction. According to Fig. 8, this preferred orientation may causes higher recoverability for cold-rolled pipe couplings, though both cold-drawn and cold-rolled pipe couplings are made from one ingot and have similar micro-morphology. However, the pipe coupling is more complicated than thin film and sheet, the exact difference between calculated and measured still needs further study.

5. Conclusions

In summary, the objective of this study is to present microstructure and properties of deformation processed NiTiNb alloy. Some important conclusions are described as follows:

1. Under hot forging, dendritic microstructure can be eliminated and eutectic structure turns into fined and dispersed. The materials become homogeneous and elongation increases. ⟨113⟩ fiber texture is induced and intensified with hot forging.
2. After cold-workings (cold-rolled and cold-drawn), the heat treatment induces static recrystallization and effectively fines grain size. Cold-drawn materials form a strong ⟨111⟩ fiber texture paralleling to the axial direction. While cold-rolled materials contains a complicated orientation, which comprises ⟨111⟩ crystal direction paralleling to the axial direction and ⟨110⟩ crystal direction aligning to the circumferential direction of tubes.
3. The recoverability of pipe coupling is affected by crystalline orientations in the circumferential direction. With ⟨110⟩ crystalline orientation arranged along circumferential direction, the pipe couplings which made by cold-rolled tubes shows greater recoverability than those made by cold-drawn tubes.

Acknowledgments

This research was supported by National 973 program under the number of 2010CB735811. The authors thank Dr. Z.W. Feng for fruitful discussion, Dr. S.C Mao for providing the EBSD tests and Shuming Wang for the XRD experimental supports.

References

1. L. Wei and Z. Xinqing, Mechanical Properties and Transformation Behavior of NiTiNb Shape Memory Alloys, *Chin. J. Aeronaut.*, 2009, **22**(5), p 540–543
2. E. Choi, H.-K. Hong, H.S. Kim and Y.-S. Chung, Hysteretic Behavior of NiTi and NiTiNb SMA Wires Under Recovery or Pre-stressing Stress. *J. Alloys Compd.*, 2012, http://dx.doi.org/10.1016/j.jallcom.2012.02.037(0)
3. K. Uchida, N. Shigenaka, T. Sakuma, Y. Sutou, and K. Yamauchi, Effects of Pre-Strain and Heat Treatment Temperature on Phase Transformation Temperature and Shape Recovery Stress of Ti-Ni-Nb Shape Memory Alloys for Pipe Joint Applications, *Mater. Trans.*, 2008, **49**(7), p 1650–1655
4. V.A. Udovenko, P.L. Potapov, S.D. Prokoshkin, I.Y. Khmelevskaya, V.Y. Abramov, and Y.V. Blinov, A Study of the Functional Properties of Alloy Ti-45%Ni-10%Nb with Wide Hysteresis of the Martensitic Transformation, *Met. Sci. Heat Treat.*, 2000, **42**(9), p 353–356
5. L. Wang, L.J. Rong, D.S. Yan, Z.M. Jiang, and Y.Y. Li, DSC Study of the Reverse Martensitic Transformation Behavior in a Shape Memory Alloy Pipe-Joint, *Intermetallics*, 2005, **13**(3–4), p 403–407
6. K. Otsuka and X. Ren, Physical Metallurgy of Ti-Ni-Based Shape Memory Alloys, *Prog. Mater. Sci.*, 2005, **50**(5), p 511–678
7. S. Miyazaki, K. Otsuka, and C.M. Wayman, The Shape Memory Mechanism Associated with the Martensitic Transformation in Ti-Ni alloys—I. Self-accommodation, *Acta Metall.*, 1989, **37**(7), p 1873–1884
8. K. Gall, H. Sehitoglu, Y.I. Chumlyakov, and I.V. Kireeva, Tension-Compression Asymmetry of the Stress-Strain Response in Aged Single Crystal and Polycrystalline NiTi, *Acta Mater.*, 1999, **47**(4), p 1203–1217
9. H. Sehitoglu, J. Jun, X. Zhang, I. Karaman, Y. Chumlyakov, H.J. Maier, and K. Gall, Shape Memory and Pseudoelastic Behavior of 51.5% Ni-Ti Single Crystals in Solutionized and Overaged State, *Acta Mater.*, 2001, **49**(17), p 3609–3620
10. K. Bhattacharya and R.V. Kohn, Symmetry, Texture and the Recoverable Strain of Shape-Memory Polycrystals, *Acta Mater.*, 1996, **44**(2), p 529–542
11. K. Gall and H. Sehitoglu, The Role of Texture in Tension-Compression Asymmetry in Polycrystalline NiTi, *Int. J. Plast.*, 1999, **15**(1), p 69–92
12. S. Miyazaki, V.H. No, K. Kitamura, A. Khantachawana, and H. Hosoda, Texture of Ti-Ni Rolled Thin Plates and Sputter-Deposited Thin Films, *Int. J. Plast.*, 2000, **16**(10), p 1135–1154
13. G.P. Cheng, Z.L. Xie, and Y. Liu, Transformation Characteristics of Annealed Ti50Ni25Cu25 Melt Spun Ribbon, *J. Alloys Compd.*, 2006, **415**(1–2), p 182–187
14. J. Tyber, J. McCormick, K. Gall, R. DesRoches, H.J. Maier, and A.E.A. Maksoud, Structural Engineering with NiTi. I: Basic Materials Characterization, *J. Eng. Mech.*, 2007, **133**(9), p 1009–1018
15. L. Zhao, Texture Development and Anisotropic Behaviour in a Ti-45Ni-5Cu (at.%) Shape Memory Alloy (Universiteit Twente, 1997)
16. H. Inoue, M. Ishio, and T. Takasugi, Texture of TiNi Shape Memory Alloy Sheets Produced by Roll-Bonding and Solid Phase Reaction from Elementary Metals, *Acta Mater.*, 2003, **51**(20), p 6373–6383
17. C.P. Frick, A.M. Ortega, J. Tyber, K. Gall, and H.J. Maier, Multiscale Structure and Properties of Cast and Deformation Processed Polycrystalline NiTi Shape-Memory Alloys, *Metall. Mater. Trans. A*, 2004, **35**(7), p 2013–2025
18. S. Mao, X. Han, M.H. Wu, Z. Zhang, F. Hao, D. Liu, Y.F. Zhang, and B. Hou, Effect of Cyclic Loading on Apparent Young's Modulus and Critical Stress in Nano-subgrained Superelastic NiTi Shape Memory Alloys, *Mater. Trans.*, 2006, **47**(3), p 735–741
19. X.Q. Zhao, X.M. Yan, Y.Z. Yang, and H.B. Xu, Wide Hysteresis NiTi(Nb) Shape Memory Alloys with Low Nb Content (4.5 at.%), *Mater. Sci. Eng., A*, 2006, **438–440**, p 575–578
20. C.S. Zhang, Y.Q. Wang, W. Chai, and L.C. Zhao, The Study of Constitutional Phases in a $Ni_{47}Ti_{44}Nb_9$ Shape Memory Alloy, *Mater. Chem. Phys.*, 1991, **28**(1), p 43–50
21. A.M. Ortega, J. Tyber, C.P. Frick, K. Gall, and H.J. Maier, Cast NiTi Shape-Memory Alloys, *Adv. Eng. Mater.*, 2005, **7**(6), p 492–507
22. Y. Sutou, T. Omori, K. Yamauchi, N. Ono, R. Kainuma, and K. Ishida, Effect of Grain Size and Texture on Pseudoelasticity in Cu-Al-Mn-Based Shape Memory Wire, *Acta Mater.*, 2005, **53**(15), p 4121–4133
23. T. Goryczka and P. Ochin, Characterization of a Ni50Ti50 Shape Memory Strip Produced by Twin Roll Casting Technique, *J. Mater. Process. Technol.*, 2005, **162–163**, p 178–183
24. X.Q. Yin, X.J. Mi, B.D. Gao, and Y.F. Li, Hot Deformation Behavior of TiNiNb Alloy, *Chin. J. Rare Met.*, 2009, **33**(6), p 921–924
25. A. Pelton, S. Russell, and J. DiCello, The Physical Metallurgy of Nitinol for Medical Applications, *JOM*, 2003, **55**(5), p 33–37
26. L. Bertheloot, P. Van Houtte, and E. Aernoudt, Texture Development in Tube Drawing, in *Proceedings Fourth Int. Conf. on Texture and the Properties of Materials (ICOTOM-4)*, Cambridge, 1975, p. 64–73
27. H. Park and D.N. Lee, Deformation and Annealing Textures of Drawn Al-Mg-Si Alloy Tubes, *J. Mater. Process. Technol.*, 2001, **113**(1), p 551–555
28. S.C. Mao, J.F. Luo, Z. Zhang, M.H. Wu, Y. Liu, and X.D. Han, EBSD Studies of the Stress-Induced B2-B19' Martensitic Transformation in NiTi Tubes Under Uniaxial Tension and Compression, *Acta Mater.*, 2010, **58**(9), p 3357–3366
29. M.R. Barnett and L. Kestens, Formation of {111} ⟨110⟩ and {111} ⟨112⟩ Textures in Cold Rolled and Annealed IF Sheet Steel, *Iron Steel Inst. Jpn. Int.*, 1999, **39**(9), p 923–929